Tellus (1996), 48A, 572–583
Printed in UK – all rights reserved

TELLUS
ISSN 0280–6495

Orogenic blocking and deflection of stratified air flow on an *f*-plane

By SIGURDUR THORSTEINSSON[1]* and SVEN SIGURDSSON[2], [1]*Icelandic Meteorological Office, Bústadavegi 9, IS-150 Reykjavik, Iceland;* [2]*Science Institute, University of Iceland, Dunhagi 3, IS-107 Reykjavik, Iceland*

(Manuscript received 22 August 1995, in final form 21 February 1996)

ABSTRACT

The stationary, finite-amplitude, orogenic disturbance of a straight barotropic air current on the rotating earth is studied numerically on the basis of quasi-static equations. Three quantifiable characteristics are defined in order to provide evaluation of the upstream flow structure: (i) the point of incipient splitting; (ii) the strength of blocking; (iii) the extent of streamline displacement. The numerical results have been used to investigate the dependence of these characteristics on the Rossby number, Ro, the non-dimensional mountain height, H, and the non-dimensional mountain shape factor, A (across-stream length/along-stream length), with the non-dimensional stability fixed. The experiments provide an indication of how the critical non-dimensional mountain height for stagnation and for splitting, respectively, depends on the Ro and A. The experiments show that the proportion of flow that goes around the mountain increases as A becomes smaller. For the cases when $\mathrm{Ro}\cdot H \gg A$, the surface-level flows upstream of the mountains are mostly or even fully diverted around it and partly blocked by the mountain. In agreement with the inferences drawn by Pierrehumbert and Wyman (1985), it is shown that for an across-stream length of mountains greater or equal to the radius of deformation, i. e., $\mathrm{Ro}\cdot H \leqslant A$, the maximum extent of the upstream influence is of the order of the radius of deformation, $\mathrm{Ro}\cdot H$. For $\mathrm{Ro}\cdot H \gg A$, this extent is limited by horizontal dispersion to a distance proportional to A.

1. Introduction

Deflection and blocking effects are of major interest when considering the interaction of mountains with the atmosphere. Does the low-level air rise over or go around the mountain, or is it held back by the mountain? Implications of vertical dispersion, Coriolis force, and horizontal dispersion for the blocking and upstream splitting are considered in this paper.

In the nonrotating case, the conditions for occurrence of flow stagnation upwind of 3-D obstacles have been considered by Smith (1980, 1989) from linearized hydrostatic equations, Smolarkiewicz and Rotunno (1990) from non-linearized non-hydrostatic equations, and Smith and Grönås (1993) from non-linearized hydrostatic equations. Furthermore, Reisner and Smolarkiewicz (1994) considered these conditions by including an idealization of surface thermal forcing.

Smith (1982) used linear theory to explain the effect of rotation on flow splitting in a three-dimensional model. According to this theory, the first effect of the rotation is to change the horizontal velocity field while the vertical velocity field remains unchanged. Moreover, the subgeostrophic flow upstream causes the air to flow around the mountain predominantly to the left, and the far field disturbance always has a low Rossby number

* Corresponding author. E-mail: siggi@rhi.hi.is.

structure even if the local Rossby number is large. The effect of rotation on blocking by a ridge was simulated in a two-dimensional numerical model by Pierrehumbert and Wyman (1985). The results of Pierrehumbert and Wyman enabled them to draw the inference that in a rotating system the Coriolis force inhibits the upstream influence by forcing an adjustment to geostrophy. Further, they inferred from scale analysis that for the case of an f-plane, at values of non-dimensional mountain height H large enough to produce nearly total low-level blocking, the dimensional length scale of the upstream influence is $L_d = Nh_m/f$, where N and h_m denote the buoyancy frequency and maximum height of the mountain, respectively. For the Alps, these figures are $h_m \approx 3$ km while $N/f \approx 100$, so that $L_d = 300$ km. Pierrehumbert and Wyman pointed out that with $L_d \ll L_y$, where L_y denotes the across-stream length of the mountain, the upstream influence is arrested at L_d and never reaches L_y. In addition, within the distance L_d the flow is subgeostrophic and the Coriolis force creates an appreciable wind along the mountain, causing the air to flow around the mountain predominantly to the left. On the other hand, they also speculated that with $L_d \gg L_y$, the upstream influence is limited by horizontal dispersion to a dimensional distance proportional to L_y. Thorsteinsson (1988; henceforth Th88) indicated how the finite amplitude, steady-state behaviour of stratified barotropic flow over circular mountains on an f-plane tends to depend strongly on the Rossby number, Ro, and the non-dimensional mountain height, H, by showing wind and temperature distribution relative to the mountain area, using an isentropic co-ordinate model. Peng et al. (1995) extended these simulations by considering elongated mountains as well as the effect of a broader scale of Rossby numbers, using a σ co-ordinate model following the terrain.

There have been some direct observations of orogenic blocking and deflection in the atmosphere. For example, Chen and Smith (1987) and Bell and Bosart (1988) gave examples of such real-life observations. Boyer et al. (1987) have carried out laboratory experiments on topographic effects in rotating stratified air with Rossby numbers from 0.05 to 0.4.

In order to expand upon these results, a series of numerical experiments have been carried out, using the Th88 model. Three quantifiable characteristics of the upstream flow structure are defined: (i) the point of incipient splitting, (ii) the strength of blocking, and (iii) the extent of streamline displacement. We investigate how the dependence of these characteristics on Ro, H, and A (across-stream length/along-stream length), as inferred from the simulations, agrees with previously proposed ideas and theory. In particular, we provide an indication of how the critical non-dimensional mountain height for stagnation and for splitting, respectively, depends on the Ro and A.

It should be noted that the model used in this paper does not include surface friction. Recent results by Bell and Bosart (1988), Xu (1990), Thorpe et al. (1993) and Xu and Gao (1995) indicate that introduction of friction can in some cases affect the results.

In Section 2, a brief description of the Th88 model is given. In Section 3, one typical simulation is presented and the above-mentioned characteristics are defined and investigated. Concluding remarks are given in Section 4 as to what extent the simulations support previous theory.

2. Model formulation

The numerical model employed in the calculations discussed in the following sections is described in Th88. Notations used below are listed in the Appendix. The set of equations governing dry-adiabatic, inviscid hydrostatic air flow on an f-plane in θ co-ordinates, including numerical divergence and Rayleigh damping terms, read

$$u_t = -\left(\frac{u^2+v^2}{2}\right)_x + vZ - m_{2x} + \kappa(\nabla\cdot\mathbf{v})_x - \mu(u-U), \tag{2.1a}$$

$$v_t = -\left(\frac{u^2+v^2}{2}\right)_y - (uZ + m_{1y}) - m_{2y} + \kappa(\nabla\cdot\mathbf{v})_y - \mu v, \tag{2.1b}$$

$$p_{t\theta} = -(up_\theta)_x - (vp_\theta)_y, \tag{2.1c}$$

$$m_{2\theta} = \Pi, \tag{2.1d}$$

where

$$Z = f + v_x - u_y = f + \xi, \quad m_2 = gz + \Pi\theta,$$

$$\Pi = c_p\left(\frac{p}{10^5\mathrm{Pa}}\right)^{R/c_p}.$$

For this set, the Montgomery potential $m(x, y, \theta, t)$

has been separated into two components as $m = m_1(y) + m_2(x, y, \theta, t)$, where the subscript $_1$ denotes a background state of geostrophically balanced flow U. The numerical divergence coefficient κ is assumed constant everywhere. The κ-terms drop out in the vorticity equation. The Rayleigh damping coefficient μ is set to be zero everywhere except in a layer near the upper boundary in which the dissipation is gradually increased to a maximum at the boundary itself.

The upper and lower boundaries are each assumed to coincide with an isentropic surface (θ_T and θ_G), and the pressure p_T at the upper boundary surface is assumed uniform and constant in time. The lower boundary condition is

$$m(x, y, \theta_G, t) = \theta_G \Pi(x, y, \theta_G, t) + g\alpha(t) h_m h\left(\frac{x}{l_x}, \frac{y}{l_y}\right) - fUy \quad \text{at } \theta = \theta_G. \tag{2.2}$$

Here, $h(\xi, \eta)$ gives the mountain profile, l_x and l_y its length and width scales, which amount to one quarter of the along-stream length and width respectively (thus $l_y = L_y/4$ where L_y is defined as in Pierrehumbert and Wyman (1985)), and h_m the crest height (assumed to be located at $(x, y) = (0, 0)$ with $h(0, 0) = 1$). The factor $\alpha(t)$ is initially zero and grows gently to unity during some finite time interval. Our attention here is restricted to the long-term, nearly steady-state solution, which should not depend strongly upon the initial development.

The initial state is assumed to be barotropic with a uniform velocity ($u = U =$ constant, $v = 0$), and with the pressure $P(\theta)$ uniform in each θ-surface. Assuming the buoyancy frequency N to be uniform everywhere, we have that

$$\Pi(P) = \Pi(p_T) + \frac{g^2}{N^2}\left(\frac{1}{\theta} - \frac{1}{\theta_T}\right). \tag{2.3}$$

As a result, the potential vorticity is at all times constant in every isentropic surface, i. e.,

$$\frac{f + v_x - u_y}{(-p_\theta)} = \frac{f}{(-P_\theta)}, \tag{2.4}$$

except in the absorbing model layer. As in Eliassen and Thorsteinsson (1984) and Th88, the mass continuity equation (2.1c) is replaced by the integrated potential vorticity equation (2.4). The model thus consists of the system of governing eqs. (2.1a), (2.1b), (2.4) and (2.1d). The inconsistency in assuming that the potential vorticity is also conserved in the absorbing layer is assumed to be of little consequence, since the results in this layer have little meaning.

Applying a constant potential temperature along the top and bottom of the model atmosphere provides both barotropic and baroclinic stability of the uniform basic current to wave disturbance (Charney and Stern, 1962).

At the side boundaries of the model, boundary conditions of the type proposed by Orlanski (1976) are employed. For steady conservative motion the real lateral streamlines $\eta(x, y)$ satisfy

$$\frac{1}{2}(u^2 + v^2) + m_2 - fUy - \kappa(\nabla \cdot \mathbf{v}) = \frac{1}{2} U^2 - fU\eta. \tag{2.5}$$

i. e., are the level curves of the Bernoulli function. The height of each isentropic surface in the x, z plane is given by

$$g\zeta(x, y, \theta) = m_2 - \theta m_{2\theta}. \tag{2.6}$$

Further details of the numerical model are discussed in Th88.

3. Description and comparison of solutions

3.1. Experimental design

In all the experiments, the mountain profile was:

$$h\left(\frac{x}{l_x}, \frac{y}{l_y}\right) = \begin{cases} \dfrac{1}{2}\left[1 + \cos\left(\dfrac{\pi}{2}\sqrt{\left(\dfrac{x}{l_x}\right)^2 + \left(\dfrac{y}{l_y}\right)^2}\right)\right] \\ \text{if } \sqrt{\left(\dfrac{x}{l_x}\right)^2 + \left(\dfrac{y}{l_y}\right)^2} < 2 \\ 0 \quad \text{if } \sqrt{\left(\dfrac{x}{l_x}\right)^2 + \left(\dfrac{y}{l_y}\right)^2} \geqslant 2. \end{cases} \tag{3.1}$$

Finite differences are used on a grid with a mesh width (distance between points where the same variables are specified) of $0.2\sqrt{2}\, l_x$, and 16 grid intervals in the vertical, of which 8 are in the inviscid layer. Despite the fact that there is not sufficient resolution in the 3-D case, this gives a good first indication. The upper absorbing layer, described in Section 2, begins at a non-dimensional height $Nz/U = 4.8$.

In order to classify the nature of flow over the family of elliptical mountain shapes (3.1), given hydrostatic air and a constant Coriolis parameter f, the following three non-dimensional parameters (Th88) are used:

$\mathrm{Ro}=U/fl_x$	the Rossby number
$H=Nh_m/U$	the non-dimensional mountain height, and
$A=l_y/l_x$	the non-dimensional mountain shape factor.

In the experiments, H varied from 0.1 to 2.0, while Ro varied from 1 to 6 and A from 1 to 6. No comparison was made with analytic calculations at $\mathrm{Ro}=\infty$, since our potential vorticity equation cannot replace the continuity equation in this case. In the integrations, the potential vorticity is conserved, which is important for flow where rotation is essential. In mountain flows evincing jumps, conservation of momentum is also important since it is one of the conditions at the jumps. The numerical scheme employed here does not yield rigorous conservation of momentum, which is a local balance. To meet this problem in all integrations the mountain height was taken to be less than the greatest value that could be used without causing the calculations to reveal jumps.

3.2. *Computed flow field*

Fig. 1 shows the result of a typical calculation, where $(\mathrm{Ro}, H, A)=(2, 2, 3)$. This field has been plotted out to the lateral boundaries. The flow is directed from left to right. The cross-section of the isentropic surfaces in the central vertical plane throughout the inviscid layer (Fig. 1a) shows the upward propagating gravity inertia waves. The x-component of the non-dimensional wind speed minimum at the surface θ_G is -0.2 and in the middle of the lowest layer $\theta_{0.5}$ it is 0.19. This is in agreement with the results concerning the very thin blocking layers noticed by, for example, Pierrehumbert and Wyman (1985) in the Alpine experiment (ALPEX). Figs. 1b, c and d show the x, y projections of real lateral streamlines (i.e., isolines of the Bernoulli function in (2.5)) at the isentropic surfaces θ_G, $\theta_{0.5}$ and $\theta_{2.5}$, respectively, in horizontal projection. The inherent three-dimensionality of the flow pattern is apparent in the low-level flow splitting around the mountain (Figs. 1b, c and d). For air originating upstream near the mountain top level, at $\theta_{2.5}$, the incoming lateral streamlines split around the wave crest slightly upstream of the mountain top. The deflection of streamlines around the mountain decreases rapidly with height. Quantification of this splitting feature is of special interest and is considered in Subsection 3.3.

3.3. *The upstream flow pattern*

The experiments confirm the result of Smith (1982) that the first effect of the rotation is to change the horizontal velocity field while the vertical velocity field is unchanged. Therefore we examine mainly the horizontal flow. As an aid in the evaluation of previous theories we define three quantifiable sub-characteristics of the upstream real wind field:

(i) the point of incipient splitting,
(ii) the strength of blocking, and
(iii) the extent of streamline displacement.

The aim of these definitions is to collect together the main results of the computed simulations and to obtain a succinct view of the upstream flow dynamics.

(i) The incipient splitting point is defined to be the non-dimensional point (x_{is}, y_{is}), where x_{is} is the lowest x-value upstream of the mountain peak, for which there are both positive and negative values of v and the difference between these values is at least one tenth of the value of the geostrophic wind. The y_{is} value is the one on the line $x=x_{is}$, where the value of v changes sign (Fig. 2). The significance of this characteristic is that x_{is} gives the length scale over which the upstream influence extends, whereas y_{is} provides a measure of the leftward air deflection around a mountain due to the Coriolis force. Note that the point of incipient splitting will not exist for all flows, but may exist even when no flow splitting occurs.

(ii) The strength of blocking is defined to be the maximum velocity deficit, $(1\text{-}u_{min})$, appearing anywhere upstream of the mountain crest. The significance of this characteristic is that $(1\text{-}u_{min})$ indicates the strength of upstream blocking as defined by Pierrehumbert and Wyman (1985). The corresponding y-value is not included in the characteristic.

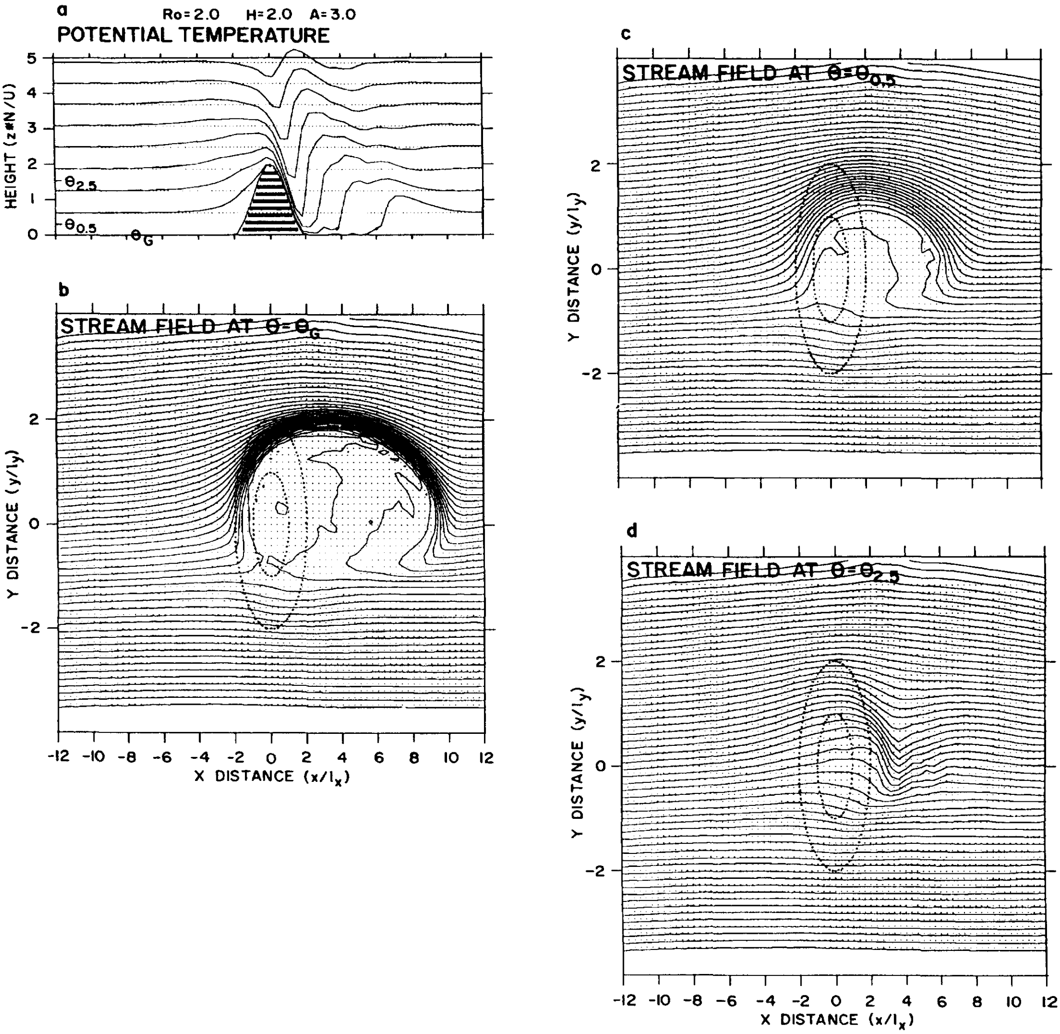

Fig. 1. Results of Experiment 1 for flow past an isolated mountain (eq. (3.1)) with (Ro, H, A)=(2, 2, 3). The dotted elliptical contours in the center of the plan view represent the height of the orography with contour interval 0.5 h_m. (a) The center plane $y=0$ showing the intersection curves with the isentropic surfaces $k=0, 1, \ldots, 8$ (heavy lines) according to eq. (2.6). (b) Horizontal projection of contours of the Bernoulli function in the θ_G surface according to eq. (2.5). (c) As for (b) except level $\theta_{0.5}$. (d) As for (c) except level $\theta_{2.5}$. Note that the height scale is expanded by a factor of two relative to the horizontal scales.

(iii) The extent of streamline displacement is defined to be the non-dimensional maximum left and right horizontal displacement (d_l,d_r), respectively, of any calculated lateral streamline at $x=0$ from their positions when no mountain is present (Fig. 2). The lateral streamlines with maximum left and right displacements need not be adjacent. The significance of this characteristic is that it provides a measure of the width scales over which the left and right mountain parallel winds extend, as well as the asymmetry of the circumflow. Further, d_l+d_r provides a measure of how great a proportion of the flow goes around the mountain. Note that when $d_l+d_r=0$ all the flow goes over the mountain whereas when $d_l+d_r \geqslant 4$ all the flow will go around the mountain, i. e., we have

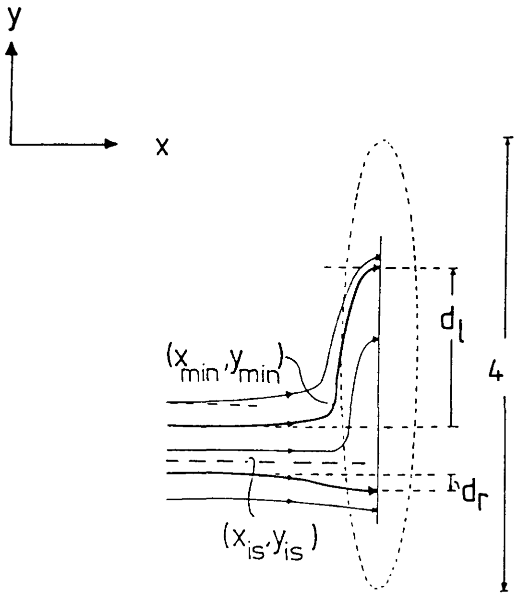

Fig. 2. Schematic diagram showing the upstream effect of the mountain in a horizontal plane. The dashed elliptic delimits the border of the topography. Plain contours are the horizontal real streamlines. (x_{is}, y_{is}) is the point of incipient splitting. (x_{min}, y_{min}) is the point of maximum velocity deficit. d_l and d_r are the maximum left and right horizontal streamline displacements.

flow splitting as defined, for example, by Smith and Grönås (1993).

Figs. 3–5 show the dependence of the three characteristics on Ro, H and A for $\theta = \theta_G$ based on the simulations for $H = 1.0$, 1.5 and 2.0, respectively. Far upstream this θ value corresponds to the height 0. Fig. 6 shows the dependence of the three characteristics on Ro and A for $\theta = \theta_{2.5}$ based on the simulations for $H = 2.0$. Far upstream this θ value corresponds to the height h_m. Note that

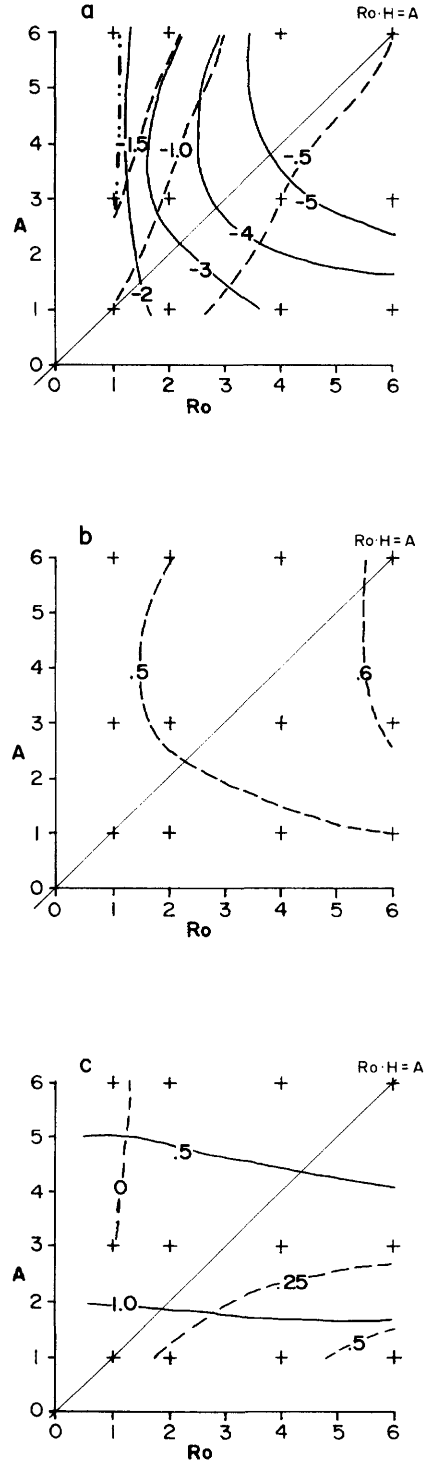

Fig. 3. Characteristic values of the upstream flow patterns drawn in the (Ro, A) plane for $H = 1$ at $\theta = \theta_G$. (a) Contours of x_{is} (normalized by l_x, solid curves) and y_{is} (normalized by l_y, dashed curves). The dashed and double dotted line marks the boundary for existence of the incipient splitting point. (b) Contours of the upstream maximum velocity deficit 1-u_{min} (normalized by geostrophic velocity, dashed curves). (c) Contours of maximum left (solid curves) and right (dashed) horizontal displacement, (d_l, d_r) respectively, (normalized by l_x and l_y, respectively) of any calculated streamlines from their equilibrium positions. The line of Ro$\cdot H = A$ is shown in the graphs a, b and c.

although no cases with $\text{Ro}=\infty$ have been calculated, the flow in these cases ($f=0$) must be symmetric about the x-axis, i.e., $y_{is}=0$, and $d_l=d_r$. This governs the shape of the curves for large Ro. The nonrotational flow has been examined in Smolarkiewicz and Rotunno (1990). The plus signs in the figures are the data points from which the contours are determined, each data point being the result of one simulation.

In the interpretation of the Figs. 3 to 6, a, b, and c it is in some cases useful to distinguish between the three regimes $\text{Ro}\cdot H \gg A$, $\text{Ro}\cdot H \approx A$ and $\text{Ro}\cdot H \ll A$. As an aid in this interpretation the line $L_d = l_y$, corresponding to $Ro\cdot H = A$ is shown. Note that $\text{Ro}\cdot H$ is the square root of the Burger number. In graphs a the bold dashed and double dotted line marks the boundary beyond which no point fulfills the criteria in the definition of the incipient splitting point. The most noteworthy results brought out by the figures are the following.

(ia) The incipient splitting point (x_{is}, y_{is}) at $\theta = \theta_G$ (Figs. 3a, 4a and 5a).

$\text{Ro}\cdot H \gg A$: At values of H large enough ($H > 1.5$) to produce nearly total low-level blocking, the x_{is} values are limited by horizontal dispersion to a non-dimensional distance proportional to A and never reach $\text{Ro}\cdot H$. This is in agreement with the conjecture of Pierrehumbert and Wyman (1985). The corresponding y_{is} values are appreciably negative, reflecting the fact that there is a stagnation point and thus an appreciable subgeostrophic u (Fig. 5b) for a sufficiently long time and sufficiently long distance. The negative y-values are consistent with the fact that the air flows around the mountain predominantly to the left. This is in accordance with discussions presented by Smith (1982) and Pierrehumbert and Wyman (1985). As an example with $\text{Ro} \leqslant 6$, $U = 10\ \text{m s}^{-1}$, $N = 10^{-2}\ \text{s}^{-1}$, $f = 10^{-4}\ \text{s}^{-1}$ and h_m equal to 2.0 km, a mountain would need to be over 200 km wide before the length scale of upstream influence reaches $L_d = 200$ km upstream.

$\text{Ro}\cdot H \sim A$: The maximum non-dimensional extent of upstream influence, x_{is}, attained by the blocked layer in the computed wave fields, scales approximately with the non-dimensional radius of deformation, $\text{Ro}\cdot H$, when H is large ($H > 1.0$).

$\text{Ro}\cdot H \ll A$: When H is large ($H > 1.5$), the upstream influence is arrested at $\text{Ro}\cdot H$ and never reaches A. As Ro decreases, the Coriolis force

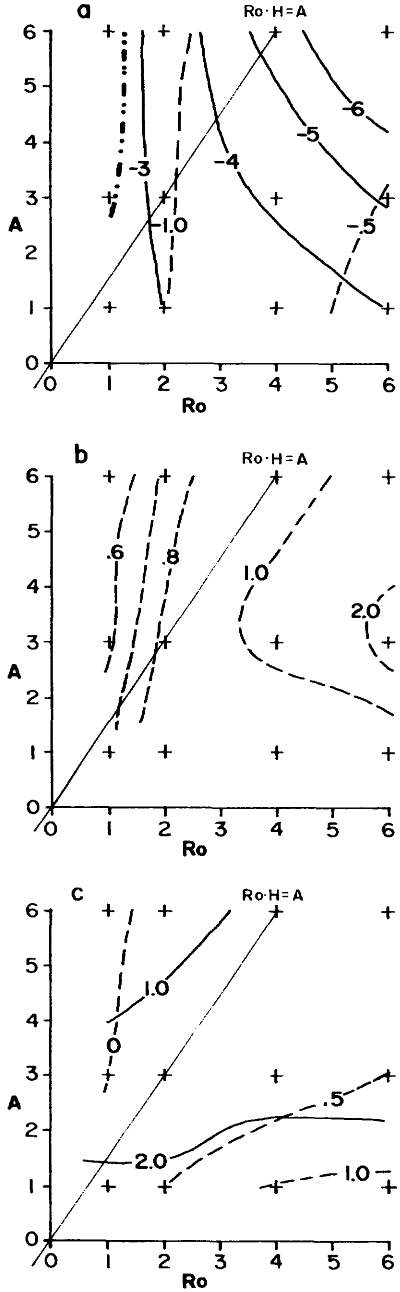

Fig. 4. As in Fig. 3, but for $H = 1.5$. In graph b the region of parameter space for which stagnant fluid in the mean flow direction is formed upstream of the mountain lies to the right of the curve labeled 1.0.

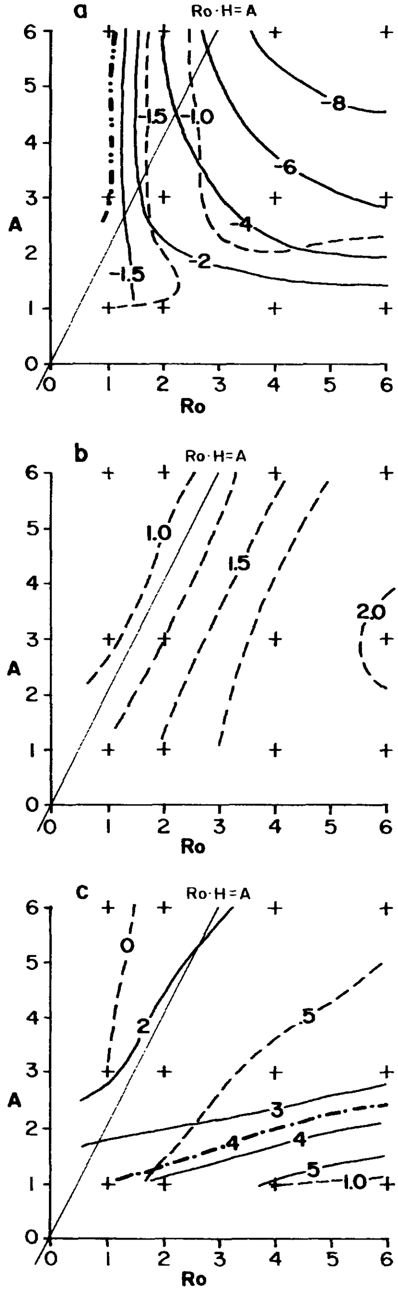

Fig. 5. As in Fig. 3, but for $H=2.0$. In graph b, the region of parameter space for which stagnant fluid in the mean flow direction is formed upstream of the mountain lies to the right of the curve labeled 1.0. The bold dashed and dotted line in graph c marks the boundary for the air flow to be fully deflected around the mountain at ground level.

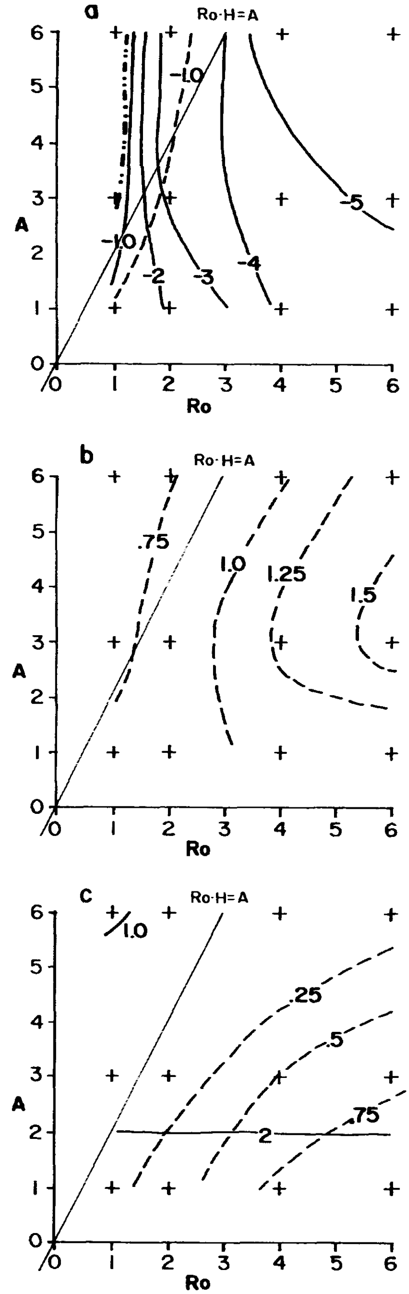

Fig. 6. As in Fig. 3, but for $H=2.0$ and level $\theta_{2.5}$. In graph b the region of parameter space for which stagnant fluid in the mean flow direction is formed upstream of the mountain lies to the right of the curve labeled 1.0.

increases the displacement of the flow splitting point toward the right, in agreement with Pierrehumbert and Wyman (1985).

(ib) The incipient splitting point (x_{is}, y_{is}) at $\theta = \theta_{2.5}$ (Fig. 6a). The location of the incipient splitting points is little affected by this increase in the potential temperature below the level of the mountain top for $\mathrm{Ro} \cdot H \ll A$ and $\mathrm{Ro} \cdot H \sim A$ but more for the regime $\mathrm{Ro} \cdot H \gg A$.

(iia) The strength of blocking $(1\text{-}u_{\min})$ at $\theta = \theta_G$ (Figs. 3b, 4b and 5b). The maximum velocity deficit is determined primarily by Ro for Ro values of order unity and $1 \leqslant A \leqslant 6$. For a small Ro, the Coriolis force inhibits the velocity deficit. Flow stagnation upwind of obstacles starts at a higher H with a decreasing Ro.

(iib) The strength of blocking $(1\text{-}u_{\min})$ at $\theta = \theta_{2.5}$ (Fig. 6b). The maximum velocity deficit is now less.

(iiia) The extent of streamline displacement (d_l, d_r) at $\theta = \theta_G$ (Figs. 3c, 4c and 5c). d_l is much greater than d_r, as had been shown in Th88 for a more restricted parameter range.

$\mathrm{Ro} \cdot H \gg A$: The d_l values are relatively insensitive to Ro. This can be deduced from the fact that d_l is determined primarily by horizontal dispersion (Pierrehumbert and Wyman, 1985). The value of d_r becomes almost zero when $\mathrm{Ro} \to 0$. The simulations show that the value of H at which the earth's rotation begins to be important is just over 1.0. The air flows upstream of the mountains do not flow over the mountains, but are mostly or even fully diverted around it and partly blocked by the mountain. This is shown by the strong left-right asymmetry of the lateral streamlines around the mountains and the pronounced flow splittings. Note that the proportion of the flow that goes around the mountains increases as A becomes smaller.

$\mathrm{Ro} \cdot H \sim A$: As Ro increases, proportionately higher A values are needed to keep the same value of d_l. This result is to be expected as when A is constant the enhanced subgeostrophic u increases d_l. When $\mathrm{Ro} \to 0$ the value of d_l decreases and the value of d_r almost becomes zero.

$\mathrm{Ro} \cdot H \ll A$: The air flows mostly over the mountains.

(iiib) The extent of streamline displacement (d_l, d_r) at $\theta = \theta_{2.5}$ (Fig. 6c). Below the mountain top level the value of d_l decreases rapidly, while d_r decreases very slowly. For small Ro values d_l is independent of Ro. For larger values of Ro, the Coriolis force limits the extent of d_l because of the smaller velocity deficit at this level.

Fig. 7 shows the results of calculations with $H = 0.1$ where the results have been multiplied by a factor of 10. The similarity between Figs. 3 and 7 indicates that for $H < 1$ the results come close to being linearly dependent on H, while a comparison between Figs. 3, 4 and 5 show that the nonlinear effects are noticeable for $H > 1$.

Finally, it should be noted that a comparison between Figs. 3b, 4b, and 5b, provides an indication of how the critical non-dimensional mountain height for stagnation in the mean flow direction depends on A and Ro at θ_G, while a comparison between Figs. 4c and 5c provides an indication of how the critical non-dimensional mountain height for flow splitting depends on these parameters at θ_G. For $H = 1.5$ and 2.0, the region of parameter space in which the air stagnates in the mean flow direction lies to the right of the curve labelled 1.0 (Figs. 4b and 5b). For $H = 1.0$, there is no such region (Fig.3b). The bold dashed and dotted line in Fig. 5c marks the boundary for flow splitting as a function of Ro and A at $H = 2$. For $H = 1.5$, there is no such boundary for the domain of the (Ro, A) parameter space considered here. It can be deduced from the graphs b and c in Figs. 3–5 that upstream stagnation in the mean flow direction can occur (at least for rotating flow in the absence of surface friction) both in the presence and non-presence of flow splitting.

According to the Smolarkiewicz-Rotunno (1989) theory of lee eddy formation, a pair of lee eddies can form in ideal non-rotating non-linear mountain wave flow. These eddies produce a new stagnation point in the lee of the mountain. The formation of these eddies in the numerical solution depends on the boundary conditions introduced where the isentropes collapse. An explicit formulation of these conditions does not seem to exist. They are, however, implicitly formed by the type of scheme chosen close to the boundary where the collapse takes place, and the final solution will thus also be dependent on that choice. In this paper the approach is taken to use the same scheme over the whole region even if the solution is physically meaningless within collapsed layers. Another possibility would be to use a weighted upstream scheme designed in such a way that values within collapsed regions never enter into the scheme. We have tried to adopt a weighted

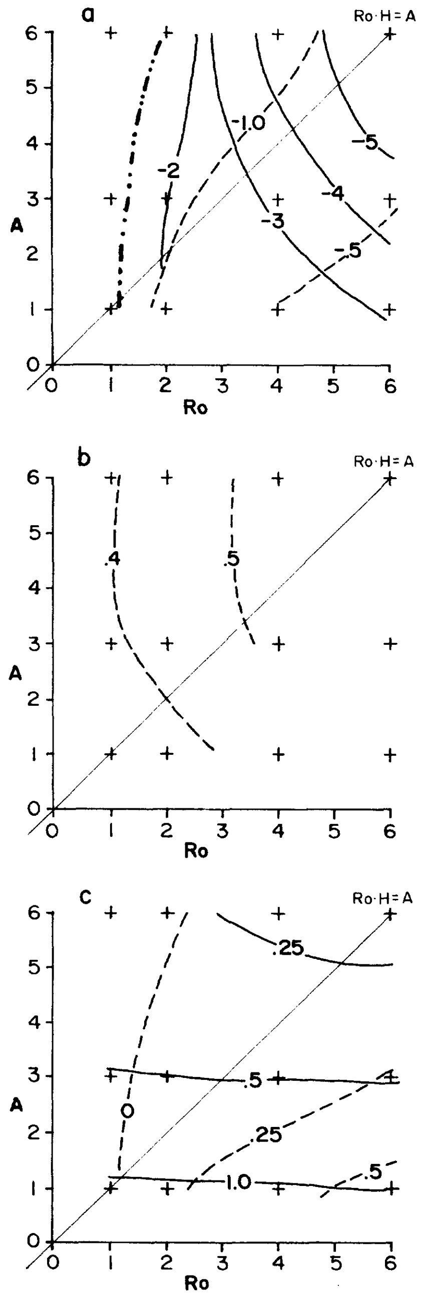

Fig. 7. As in Fig. 3, but for $H=0.1$. Results have been multiplied by a factor of 10.

upstream scheme, developed by Piotr Smolarkiewicz for a grid which is non-staggered both in space and time, to our staggered grid. The resulting calculations indicated, however, that while the problem with space staggering could be dealt with, the time staggering led to instabilities caused by limited coupling between the two time levels that seem to be difficult to overcome. We have thus had to abandon such an approach.

Another important question in stratified flow is when gravity wave breaking begins above the mountain. Like flow splitting, wave breaking begins with the formation of a stagnation point. In these low Ro-number experiments stagnation aloft was not found. This fact, together with the fact that no wave breaking was observed in ALPEX and PYREX, may indicate a very small contribution, if any, to wave breaking over terrain on the scale of the Alps and the Pyrenees. While it must be kept in mind that overturning isentropic surfaces is not allowed for in the model design used in this paper one would expect the numerical solution to break down under such situations.

4. Concluding remarks

This investigation has dealt with mesoscale atmospheric response to topographic forcing at hydrostatic scales. Three quantifiable characteristics have been proposed (Fig. 2) in order to give a concise description of the upstream patterns of flow: (i) the point of incipient splitting, (ii) the strength of blocking, and (iii) the extent of streamline displacement. The aim of the experiments presented in this paper has been to investigate how the dependence of these characteristics on the Rossby number, Ro, the non-dimensional mountain height, H, and the non-dimensional mountain shape factor, A (across-stream length/along-stream length), with the non-dimensional stability fixed (Figs. 3–7) agrees with previously proposed ideas and theory.

In particular we provide an indication of how the critical non-dimensional mountain height for stagnation in the mean flow direction (Figs. 3b, 4b and 5b) and for flow splitting (Figs. 4c and 5c), respectively, depends on the Ro and A at the ground. It can be deduced from these graphs that upstream stagnation in the mean flow direction (i.e., blocking) can occur (at least for rotating flow in the absence of surface friction) both in the presence and non-presence of flow splitting.

The experiments show that in the regime $1 \leqslant A \leqslant 6$, $1 \leqslant \mathrm{Ro} \leqslant 6$, the deflection by mountains is more sensitive to the value of A than to the value of Ro, while the blocking is more sensitive to the value of Ro than to the value of A. The proportion of flow that goes around the mountain increases as A becomes smaller. For the cases when $\mathrm{Ro} \cdot H \gg A$ the surface-level flows upstream of the mountains are mostly or even fully diverted around it and partly blocked by the mountain.

As already shown by Smith (1982) and Th88, it can be seen that, if the Rossby number is of the order of 1 for a sufficiently large H and A, blocking of the air on the windward right side develops, and most of the low-level air goes around the mountain on the windward left side in the Northern Hemisphere. It can therefore be concluded that, at a Rossby number even as high as 6 and with H greater than 1.5, the earth's rotation has a marked influence upon the upstream flow pattern at ground level, causing the low-level air to flow around the mountain predominantly on the left side. This is in accordance with discussions presented by Smith (1982) and Pierrehumbert and Wyman (1985). As already indicated by the experiments in Th88, it is seen that flow stagnation upwind of obstacles starts at a higher H with decreasing Ro. In agreement with the inferences drawn by Pierrehumbert and Wyman (1985), it can be concluded that for mountains with a non-dimensional across-stream length of greater than or equal to the radius of deformation, i. e., $\mathrm{Ro} \cdot H \leqslant A$, the maximum extent of the upstream influence is of the order of the radius of deformation, $\mathrm{Ro} \cdot H$. For $\mathrm{Ro} \cdot H \gg A$, on the other hand, this extent is limited by horizontal dispersion to a distance proportional to A.

5. Acknowledgements

This research has been supported by the Icelandic Council of Science. The first author is also grateful for the hospitality provided by the Geophysical Fluid Dynamics Laboratorium (GFDL), Princeton University, where this research was initiated. Further, he wishes to thank Ray T. Pierrehumbert for fruitful discussions and helpful suggestions regarding the flow characteristics. The helpful comments by Arnt Eliassen, Ronald B. Smith, Piotr K. Smolarkiewicz and an anonymous reviewer are also appreciated.

6. Appendix:

List of symbols

A	aspect ratio of the horizontal scales of the mountain in y and x directions, respectively
c_p	$=1004\ \mathrm{m^2\ s^{-2}\ K^{-1}}$ specific heat capacity at constant pressure
d_l, d_r	non-dimensional maximum left and right horizontal streamline displacement, respectively
f	Coriolis parameter
g	$=9.8\ \mathrm{m\ s^{-2}}$ acceleration of gravity; suffix indicating geostrophic
G	suffix indicating lower boundary
h	shape and location of mountain
h_m	maximum height of mountain
H	$=Nh_m/U$ non-dimensional height of mountain
k	numbering of θ-surfaces ($k=0$ at the ground)
L_d	$=Nh_m/f = H \cdot \mathrm{Ro} \cdot l_x$
l_x	one quarter along-stream length of elliptical mountain
l_y	one quarter across-stream length of elliptical mountain
L_y	across-stream length of elliptical mountain
m	$=gz+\theta\Pi(p)$ Montgomery potential; m_1 and m_2 defined in Section 2
M	initial equilibrium values of m
N	buoyancy frequency
p	pressure
P	initial equilibrium values of p
q	potential vorticity
R	$=287\ \mathrm{m^2\ s^{-2}\ K^{-1}}$ specific gas constant
Ro	$=U/fl_x$ Rossby number
t	time
T	temperature; suffix indicating upper boundary
u, v	Cartesian components of horizontal velocity
u_{min}	minimum value of x-value velocity upstream of the mountain

U	initial equilibrium values of u
x, y	horizontal Cartesian coordinates
x_{is}	defined in Subsection 3.3
x_{min}	x-coordinate of the maximum velocity deficit point
y_{is}	the value on the line $x=x_{is}$, where the value of v changes sign
z	height
Z	$=f+\xi=f+v_x-u_y$
$\eta(x, y)$	lateral streamline displacement
ζ	vertical streamline displacement
θ	$=c_p T/\Pi(p)$ potential temperature
θ^*	$=c_p/U^2$ unit for potential temperature
θ_G	constant potential temperature of the lowest isentropic surface coinciding with the ground
κ	horizontal diffusivity coefficient
μ	Rayleigh friction coefficient
ξ	relative vertical vorticity
$\Pi(p)$	$=c_p\left(\dfrac{p}{10^5\ \mathrm{Pa}}\right)^{R/c_p}$ Exner function

REFERENCES

Bell, G. D. and Bosart, L. F. 1988. Appalachian cold-air damming. *Mon. Wea. Rev.* **116**, 137–161.

Boyer, D. L., Davies, P. A., Holland, W. R., Biolley, F. and Honji, H. 1987. Stratified rotating flow over and around isolated three-dimensional topography. *Phil. Trans. R. Soc. Lond. A* **322**, 213–241.

Charney, J. and Stern, M. E. 1962. On the stability of internal baroclinic jets in a rotating atmosphere. *J. Atmos. Sci.* **19**, 159–172.

Chen, W. -D. and Smith, R. B. 1987. Blocking and deflection of airflow by the Alps. *Mon. Wea. Rev.* **115**, 2578–2597.

Eliassen, A. and Thorsteinsson, S. 1984. Numerical studies of stratified air flow over a mountain ridge on the rotating earth. *Tellus* **36A**, 172–186.

Orlanski, I. 1976. A simple boundary condition for unbounded hyperbolic flows. *J. Comput. Phys.* **21**, 251–269.

Peng, M. S., Li, S., Chang, S. W. and Williams, R. T. 1995. Flow over mountains: Coriolis force, transient troughs and three dimensionality. *Q. J. R. Meteorol. Soc.* **121**, 593–613.

Pierrehumbert, R. T. and Wyman, B. 1985. Upstream effects of mesoscale mountains. *J. Atmos. Sci.* **42**, 977–1003.

Reisner, J. M. and Smolarkiewicz, P. K. 1994. Thermally forced low Froude number flow past three-dimensional obstacles. *J. Atmos. Sci.* **51**, 117–133.

Smith, R. B. 1980. Linear theory of stratified hydrostatic flow past an isolated mountain. *Tellus* **32**, 348–364.

Smith, R. B. 1982. Synoptic observations and theory of orographically disturbed wind and pressure. *J. Atmos. Sci.* **39**, 60–70.

Smith, R. B. 1988. Linear theory of hydrostatic flow over an isolated mountain in isosteric coordinates. *J. Atmos. Sci.* **45**, 3889–3896.

Smith, R. B. 1989. Mountain-induced stagnation points in hydrostatic flows. *Tellus* **41A**, 270–274.

Smith, R. B. and Grönås, S. 1993. Stagnation points and bifurcation in 3-D mountain airflow. *Tellus* **45A**, 28–43.

Smolarkiewicz, P. K. and Rotunno, R. 1989. Low Froude number flow past three-dimensional obstacles. Part I: Baroclinically generated lee vortices. *J. Atmos. Sci.* **46**, 1154–1164.

Smolarkiewicz, P. K. and Rotunno, R. 1990. Low Froude number flow past three-dimensional obstacles. Part II: Upwind flow reversal zone. *J. Atmos. Sci.* **47**, 1498–1511.

Smolarkiewicz, P. K., Rasmussen, R. M. and Clark, T. L. 1988. On the dynamics of Hawaiian cloud bands: Island forcing. *J. Atmos. Sci.* **45**, 1872–1905.

Thorpe, A. J., Volkert, H. and Heimann, D. 1993. Potential vorticity of flow along the Alps. *J. Atmos. Sci.* **50**, 1573–1590.

Thorsteinsson, S. 1988. Finite amplitude stratified air flow past isolated mountains on an *f*-plane. *Tellus* **40A**, 220–236.

Xu, Q. 1990. A theoretical study of cold air damming. *J. Atmos. Sci.* **47**, 2969–2985.

Xu, Q. and Gao, S. 1995. An analytic model of cold air damming and its application. *J. Atmos. Sci.* **52**, 353–366.